Nanoscale

PAPER

View Article Online
View Journal | View Issue

Cite this: *Nanoscale*, 2025, **17**, 2793

Self-limiting selective phase separation of graphene oxide and polymer composite solution†

Feifan Chen, [a] Lidan Wang,[a] Kaiwen Li,[a] Rui Guo, [a] Yicong Qin,[a] Chenwei Shen,[a] Yingjun Liu,[a,b] Zhen Xu*[a,b] and Chao Gao *[a,b]

Received 7th November 2024,
Accepted 6th January 2025

DOI: 10.1039/d4nr04636f

rsc.li/nanoscale

Homogeneous mixtures undergo phase separation to generate rich heterogeneous structures as well as enable complex physiological activity and delicate design of artificial materials. Beyond free space, the strong coupling between migrating components and spatial confinement plays a crucial role in determining the essential spatial compartment of phase separation, warranting further continuous exploration. Herein, we report the selective phase separation (SPS) behavior of polymers under a mobile two-dimensional (2D) confinement by graphene oxide (GO) sheets. The selection of a poor solvent triggers the occurrence of SPS in a homogeneous solution of GO and polymers. We reveal that the self-limiting spatial confinement of GO sheets leads to the migration of polymers to form independent and continuous phase in 2D confinement. We examine the quantitative rule of size and continuity of polymer phases in correlation with solvent properties and solute constitutes. The observed SPS allows the facile generation of heterogenous nanostructures in GO/polymer composites. We initiate a SPS wet-spinning to fabricate radial heterogenous fibrous graphene composite fibers with ultrahigh elongation at break and superior flexibility. The observed SPS can inspire more exceptional phase separation behaviors under mobile 2D confinement and offers a facile method to delicately design 2D heterogeneous nanostructured materials.

Introduction

Phase separation of a homogenous multiple component system is a fundamental principle underlying biological activities,[1,2] self-assembly[3,4] and material processing.[5–8] For phase separation activated by external conditions, such as temperature, pressure and solution properties, simultaneously mixing components leads to their spatial redistribution and separation into different phases, underpinning the condensation of biomolecules and the formation of extremely rich structures for tailored design materials. For example, delicate nanostructures obtained *via* phase separation in the self-assembly form have been extensively used for lithography techniques,[9–11] 3D printing,[12,13] organic electronic devices,[14–17] separation membranes,[18–21] electrochemical energy storage[22] and batteries.[23–27] Phase separation enables a bicontinuous structure and simultaneously promotes the strength and toughness of gels and nanocomposites.[28–31] Apart from phase separation in free space, phase separation in confined space has emerged as a complicated but important phenomenon in realistic circumstances but is yet to be completely explored.

For confined phase separation, external spatial confinement can affect thermodynamic and kinetic processes,[32–34] either through anchoring and repulsion at interfaces or obstructing the diffusive separation of components. Previous studies have revealed that confined spatial interfaces generate a dominating influence in dynamics and render intriguing phase separation phenomena.[35–38] For example, phenomena such as spinodal decomposition waves close to the interface,[39] quenched double phase separation,[40] and coarsening coexisting phases through a wetting effect[41,42] have been observed. Surface constraints can meditate phase separation to turn isolated droplets into continuous phases.[43] Recently, two-dimensional sheets have been extensively integrated with various components to yield complex assemblies and materials.[44–47] In their mixing system, 2D sheets with an ultimate surface nature can be considered seamless atomic barrier interfaces. The existence of mobile 2D sheets should give a significant information on phase separation, yet the phenomenon remains unclear.

[a]*MOE Key Laboratory of Macromolecular Synthesis and Functionalization, Department of Polymer Science and Engineering, Key Laboratory of Adsorption and Separation Materials & Technologies of Zhejiang Province, Zhejiang University, Hangzhou 310027, China*
[b]*Shanxi-Zheda Institute of Advanced Materials and Chemical Engineering, Taiyuan 030000, China*

† Electronic supplementary information (ESI) available. See DOI: https://doi.org/10.1039/d4nr04636f

Herein, we report the self-limiting SPS behaviour of polymers in solution meditated by the mobile confinement of model 2D GO sheets. The impermeability of GO sheets forces the migration of polymers to be the dominating separation process to form specific sandwiched structures. The quantitative rule of size and continuity of polymeric phases correlates with solvent properties and solute constitutes. We propose SPS wet-spinning to continuously fabricate radial heterogenous fibrous graphene composite fibers, which exhibit higher elongation at break and superior flexibility than homogeneous fibers. The self-limiting SPS can inspire additional exotic phase separation behaviours under the meditation of 2D sheets and offer a facile method to delicately design and fabricate a heterogeneous nanostructure of 2D materials.

Experimental

Materials

Aqueous GO dispersions were purchased from Hangzhou Gaoxi Technology Co. Ltd. Polyethylene oxide (PEO), polyvinyl alcohol (PVA) and dimethylacetamide (DMAC) were purchased from Shanghai Macklin Biochemical Co., Ltd. Cellulose nanocrystals (CNCs) were purchased from Aladdin Biochemical Technology Co., Ltd. Polystyrene (PS) and polyacrylonitrile (PAN) were acquired from Sigma-Aldrich Co., Ltd. Other reagents were purchased from Sinopharm Chemical Reagent Co., Ltd and used as-received.

Preparation of GO solution, polymer solution and GO/polymer solution

To obtain a GO/DMAC solution for the experiment, water in aqueous GO dispersion was replaced by DMAC *via* a repeating centrifugation method for at least five times to obtain GO/DMAC liquid crystal dispersion of 20 mg mL^{-1}.

To prepare the polymer solution, different polymer powders were dispersed. PS was dispersed in DMAC with a concentration of 10 mg mL^{-1} and stirred for 4 h at 60 °C. PEO powder was dispersed in DMAC with a concentration of 10 mg mL^{-1} and stirred for 4 h at 60 °C. PVA powder was dispersed in DMAC with a concentration of 10 mg mL^{-1} and stirred for 5 h at 90 °C. PAN powder was dispersed in DMAC with a concentration of 10 mg mL^{-1} and stirred for 12 h at 25 °C. CNC powder was dispersed in deionized water with a concentration of 10 mg mL^{-1} and stirred for 4 h at 25 °C.

To prepare the GO/polymer solution, a polymer solution was added to the GO solution while being homogeneously stirred. The concentration and composition ratio of the GO/polymer solution can be adjusted.

Fabrication of GO/PS observation sample

The GO/PS homogeneous solution was spin-coated onto a glass substrate to get a liquid film under a nitrogen atmosphere to prevent exposure to moisture. The spin-coated GO/polymer film was placed in EA quickly to generate SPS and then in ethanol to freeze the SPS structure.

Fabrication of SPS-GO/PEO fibers and homogeneous GO/PEO fibers

As per the established SPS, a GO/PEO spinning dope was injected *via* a spinneret (100 μm diameter) into coagulation baths containing EA. For fabricating homogeneous GO/PEO fibers, the GO/PEO spinning dope was injected into coagulation baths containing a mixture of EA and ethanol. SPS-GO/PEO fibers and homogeneous GO/PEO fibers were continuously solidified and collected onto graphite rollers.

Characterizations

The static observation of SPS was conducted by a polarizing optical microscope (OM, Nikon, LV100N POL). The 3D structures of SPS observation samples were observed using a confocal laser scanning microscope (CLSM, Zeiss LSM 900). The morphology and microstructure of SPS observation samples, fibers and films were characterized by scanning electron microscopy (SEM) inspections on a Hitachi S4800 field emission system. Polymer migration and graphene stacking were characterized using a transmission electron microscope (TEM, Hitachi 7800). X-ray diffraction (XRD) patterns were collected on an X'Pert Pro (PANalytical) diffractometer using a monochromatic Cu 17 Kα1 radiation (λ = 1.5406 Å) at 40 kV. The homogeneity of the solution was confirmed using dynamic light scattering (DLS, ALV/CGS-3). The retention of the polymer was characterized by thermogravimetric analysis (TGA, SDT Q600) and Fourier transform infrared spectroscopy (FTIR, Nicolet 6700). Tensile stress–strain tests were conducted using a Keysight T150 UTM and Instron 2344 with a gauge length of 5 mm and extension rate of 1.67×10^{-2} s^{-1}. At least three samples of each fiber type were tested to measure the average mechanical properties and standard deviations.

Results and discussion

SPS of GO/polymer solutions

Aggregation of GO/polymer solutions has been widely used to prepare complex structure and materials with the homogenous distribution of both GO and polymer, such as strong composite papers,[48–50] fibers[51–54] and aerogels.[55–57] Generally, this aggregation is triggered by a poor solvent for both the GO and polymer. We aim to study the new possible phase separation behavior as the mixture system interacts with the solvent, which is only poorly selective for one component but highly selective for other. As a model experimental system, we started from the homogeneous mixture of GO and PS in the common good solvent (DMAC) and monitored the phase separation as immersed into ether acetate (EA), which is a good solvent for PS but a poor solvent for GO. We used OM to directly monitor the SPS process because the movement of PS chains occurs in the interlayer space between GO sheets.

Different phase separation behaviors in EA and ethanol (Fig. 1 and 2) can be seen in the GO/PS spin-coated thin film (Fig. 2a). In the GO/PS solutions, PS chains are homogenously distributed in the GO interlayer gallery. EA is the poor solvent

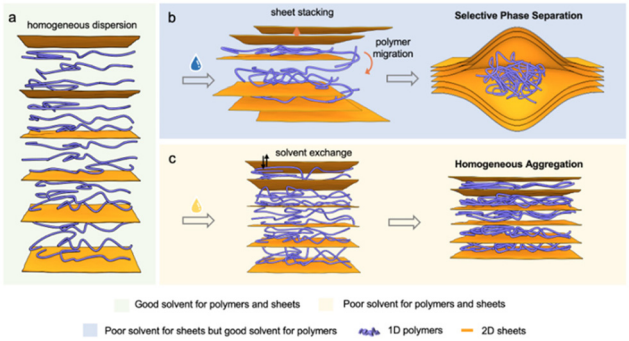

Fig. 1 Schematic of SPS and homogeneous aggregation. (a) Homogeneous dispersion of polymers and sheets in good solvent and polymer chains homogeneously distributed in the interlayer gallery. (b) The occurrence of SPS by introducing a second solvent, which is poor for sheets but good for polymers, in which 2D sheets selectively self-stack to form a network while polymer chains migrated along with their good solvent. (c) The introduction of a poor solvent for both sheets and polymers triggers homogenous aggregation *via* solvent exchange.

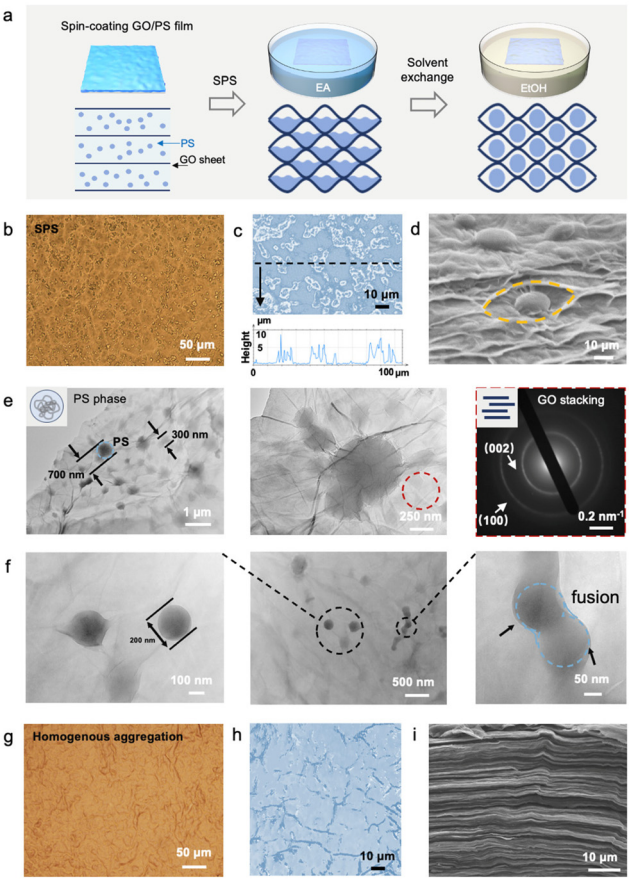

Fig. 2 Validation of the occurrence of SPS (a) schematic of the model sample preparation of SPS. Spin-coated thin GO/PS solution layer is quickly immersed into EA to trigger SPS, and then in ethanol to freeze the SPS structure for examination. (b–f) OM (b), CLSM (c), SEM (d) and TEM (e and f) images of SPS-GO/PS. OM (g), CLSM (h) and SEM (i) images of homogenous aggregation GO/PS.

for GO and can cause the stacking contact of GO sheets to drive the solvent out of the interlayer (Fig. 1b and S1†). Upon contact with EA, which is good for PS but poor for GO, we observed a typical phase separation in which GO and PS selectively aggregate with themselves (Fig. 2b–d), which is coined as SPS. Based on the phenomena in neat GO and GO/PS cases, the SPS process can be triggered by the stacking of GO sheets to squeeze the interlayer PS/EA solution to form selective aggregations. However, for poor solvents such as EA/ethanol, homogenous aggregation occurred and both GO and PS simultaneously aggregated to form a homogenous sandwiched laminate solid after drying (Fig. 1c) and uniformly appeared under OM (Fig. 2g), CLSM (Fig. 2h) and laminated section morphology (Fig. 2i).

To verify the GO stacking in SPS, we directly tracked the process by OM. The appearance of semi-transparent planar aggregation with many folds from the blank transparent solutions denotes GO stacking (Fig. 2b, c and Fig. S2†). The SEM cross-section morphology demonstrates that the wrinkled GO stacks sandwich the aggregated PS granules (Fig. 2d), which is distinct from the compact stacked layered structure formed by homogenous aggregation (Fig. 2i). Closer TEM inspection reveals that GO sheets are stacked together by a random layer order as can be seen by the diffused diffraction circle pattern in the selected area electron diffraction (SAED) results (Fig. 2e and S3†).

To investigate the selective aggregation of the PS phase, we used OM, SEM and TEM to examine the morphology of aggregated PS in GO laminates (Fig. 2b–f). The OM image shows that the PS aggregate forms granules with a smooth shape (Fig. 2b and Fig. S4†) and a wide diameter range from 3 to 8 μm, which corresponds to the separated PS solution in SPS (Fig. 2c). In the SEM section, PS granules were wrapped by flexible GO sheets. In addition to these large micron-sized granules, we found the PS aggregate in SPS at the nanoscale and captured the microscale migration process of the PS phase by TEM. For the GO laminates, smaller granules with a diameter from 200 to 700 nm can be detected (Fig. 2e). Closer inspection captures the fusion process of SPS, which shows that the PS solution migrates in the stacking channel (drain trace around PS granules) and fuses together to form multiscale aggregates in the GO laminates (Fig. 2f and Fig. S5†). For phase separation, the migration of phases acts as a dynamic factor to influence the final morphology.[58,59] In SPS, GO stacking drives the aggregation of the PS phase but stops its free movement, resulting a wide size distribution of PS granules from 10 μm to 200 nm.

Geometric rule of SPS

In the model GO/PS system, we reported that SPS can generate two distinct phase separation structures of PS, which are independent droplet and continuous states (OM image in Fig. 3a) determined by the ratio between GO and PS. For the droplet state, the diameter increases from 1 to 12 μm as the GO/PS solution concentration increases from 0.1% to 1%. In the usual phase separation of the polymer solution, as the concen-

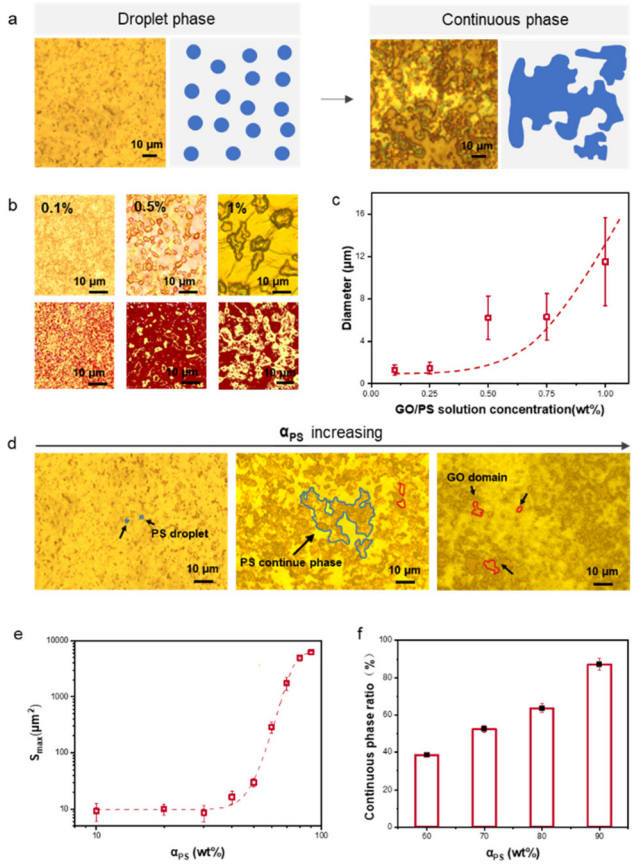

Fig. 3 Geometric rule of SPS. (a) Two phase states of SPS: droplet and continuous phases. (b) The trend of the diameter changes with the solution concentration of GO/PS. (c) Diameter as a function of GO/PS solution concentration. (d) SPS transition from the droplet phase to the continuous phase. (e) Maximum cluster area as a function of the proportion of PS (α_{PS}). The percolation threshold is about 0.6. (f) Continuous phase ratio as a function of α_{PS}.

tration reduces, the motion of the polymer chains hinders the dynamic process of phase separation, and therefore the size of the aggregated phase reduces.[60,61] However, the SPS exhibits a reverse trend that PS granules grow with the increasing concentration of the GO/PS solution (Fig. 3b, c and Fig. S6, S7†), which is mainly attributed to the dominating confinement of GO sheets. As concentration increases, the stacking of GO sheets can drive the confined PS liquid phase with a higher concentration to fuse together to become larger droplets, unlike the retarded movement of polymer chains in the usual phase separations.

We tracked the evolution process from independent droplets to a continuous phase by tuning the proportion of GO/PS while maintaining a constant solid content (1 wt%) under OM observation. Fig. 3d captures the typical phase state from independent droplet (the proportion of PS, α_{PS} of 10%), interconnecting PS domains (α_{PS} of 50%), to a completely continuous PS network with independent GO domains (α_{PS} of 90%). In polymer composite materials, a traditional geometric concept of networks has the percolation threshold, at which nanofillers become continuous across the microscopic length. We quantitatively measured the maximum cluster area of PS phases and detected a transition proportion of PS containing around 60%, which is close to 59.2% of the theoretic percolation threshold of the 2D lattice,[62] as can be seen in Fig. 3e. We defined the phase after this critical value (α_{PS} = 0.6) as the PS continuous phase. After the percolation threshold, the PS maximum cluster size demonstrated an increasing trend with the increase in α_{PS} from 60% to 90% (Fig. 3f and Fig. S8, S9†).

The generality of SPS in other graphene-polymer system

In addition to the selective precipitation for GO sheets, the SPS process can happen for the selective aggregation of polymers (Fig. 4a). We immersed the spin-coated GO/PAN liquid film into deionized water, which is a poor solvent for PAN but good for GO. At the typical α_{PAN} of 50%, the liquid film turned into floating films on the air/water interface (Fig. 4b). Under OM and TEM, the aggregated PAN binds GO sheets to form the film and

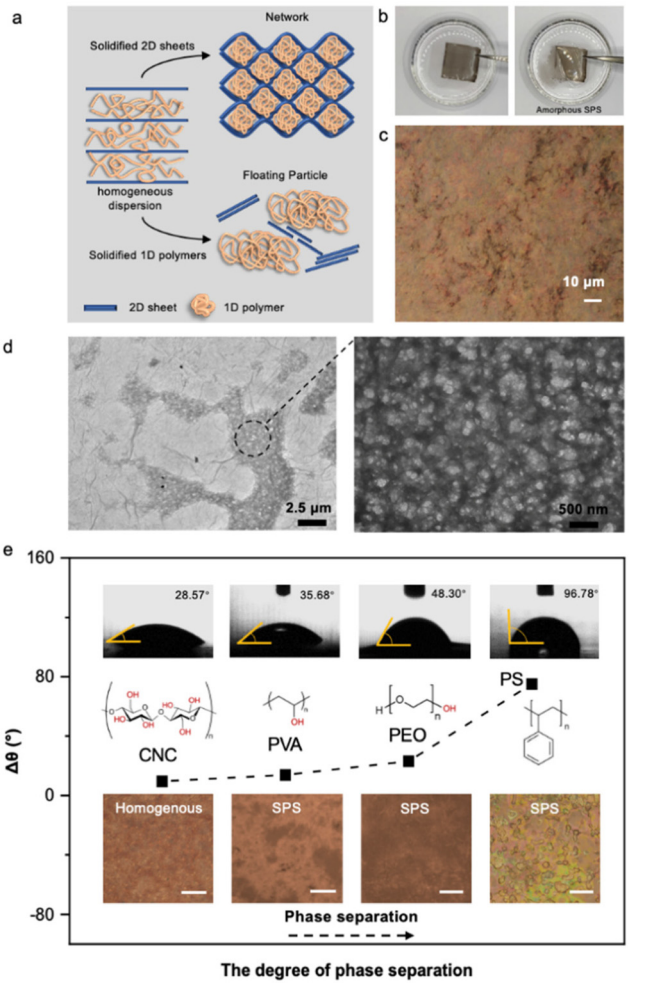

Fig. 4 SPS for the GO polymer mixing system. (a) Schematic of SPS for poor solvent either for polymer or GO. (b) The SPS process of the GO/PAN film. (c) The OM image of the SPS-GO/PAN film. (d) TEM image of the SPS-GO/PAN film. (e) The relationship between the contact angle and the degree of SPS, scale bar is 20 μm.

exhibits an amorphous network structure (Fig. 4c and d). In the SPS for the polymer, the dominating separation is the aggregation of polymers to form the network backbone, which is distinct from the GO backbone in the case of SPS for GO (Fig. 3).

To examine the generality of SPS in the GO polymer system, we selected CNC, PVA and PEO as a polymer component within the same EA as a poor solvent to trigger SPS for GO (Fig. 4e). We observed that this series of polymers exhibits a similar SPS behavior. In particular, the phase separation size increases with the hydrophobicity of polymers with increase in water contact angle, which could provide a method to tune the phase separation structure *via* select polymer structures (Fig. S10 and Table S1†).

The application of SPS in wet-spinning

The fundamental SPS mechanism guides us to propose a SPS spinning method to prepare graphene-based fibers with a distinctive hierarchical structure in the interior of fibers other than the previous homogenous structures.[51–54]

Starting from the homogeneous liquid crystalline mixture of GO and PEO, which confirmed by OM and DLS (Fig. S11–13†), we changed the coagulation bath to SPS (EA) and the SPS spinning method yielded SPS fibers with a hierarchical phase separated structure (Fig. 5a and S14†). As expected, the typical SPS fiber has a folded graphene lamellar structure with isolated PEO microscale islands, different from the homogenous fiber coagulated in the mixture of EA/ethanol (Fig. 5b and Fig. S15†). XRD was conducted to help interpret the mechanism of SPS and the XRD spectrum confirmed that the PEO aggregates together (120 and 112 facet peaks) in the SPS fiber along with homogenous aggregation in the usual fiber (the expanded interlayer of 001 GO peak), as can be seen in Fig. 5c. We used TGA and FTIR to verify the retention of polymer in the SPS fiber. For SPS fibers, TGA curves have two decompositions at about 200 °C and 400 °C and lowers residue content than pure GO fibers, which shows the presence of PEO (Fig. S16†). The distinction of the FTIR curves of pure GO and SPS fibers and the similarity of the FTIR curves of pure PEO and SPS fibers indicates the existence of PEO in SPS fibers (Fig. S17†). The retention of PEO in SPS fibers is attributed to a short time immersion (~5 s) in the spinning process, which avoids the diffusion of PEO into EA. However, repeating washing by EA can soak out all PEO in the aggregation (Fig. S18 and S19†), denoting by the migration of PEO in the SPS process.

The SPS graphene-based fiber exhibited an extraordinary flexibility, unlike the usual brittleness of graphene-based fibers.[63–65] As can be seen in Fig. 5d, the SPS graphene fiber can be stretched to a high strain up to 77%, much higher than that of homogenous fibers (Fig. S20 and Table S2†). This contrast can be attributed to the hierarchical structure of the SPS fiber, which greatly relieves the fatal stress concentration in the lamellar structures. The SPS graphene fiber can be fastened into a tight knot without any breakage, showing a much better flexibility than the usual homogenous graphene fibers (Fig. 5e, f and Fig. S21, S22†).

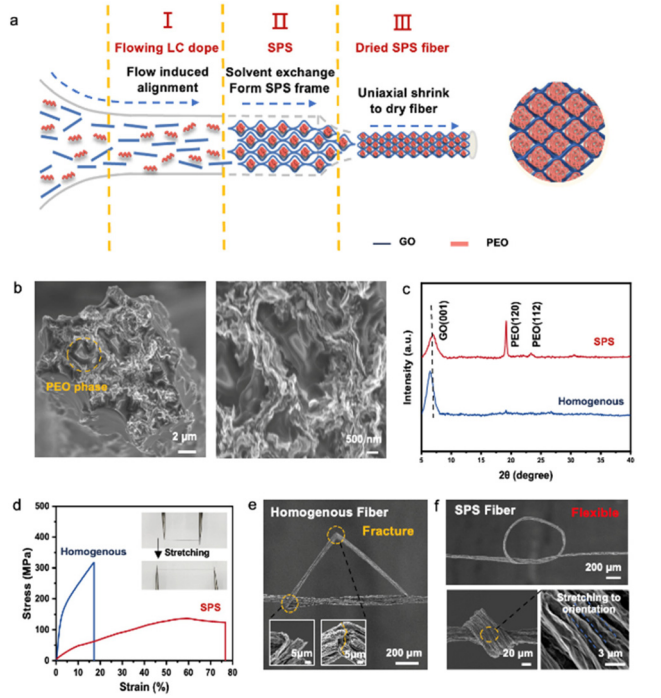

Fig. 5 Structures and mechanical performances of SPS fibers. (a) Schematic of SPS spinning, in which the coagulation bath is changed to poor solvent only for GO. (b) Fracture section of SPS fibers. (c) XRD of GO/PEO fibers. (d) Tensile curves of homogenous GO/PEO fibers and SPS fibers. (e) SEM images of homogenous GO/PEO fibers. (f) SEM images of SPS fiber knots.

Conclusions

In this work, we investigated the selective phase separation behaviour of the mobile 2D sheet-confined solution system. We revealed the basic self-limitation mechanism of SPS in the model GO/polymer system, which behaves distinctly from the usual polymer solution system. The SPS behaviour can initiate a profound understanding of the complex phase behaviour in the confined solution systems. As a fundamental rule, phase separation has widely guided the design and fabrication of delicate multiscale structures and useful materials. Similarly, SPS can be used to design complex 2D hybrid structure in a simple manner by selecting solvent properties from the homogenous liquid mixtures, which has been seldomly tried previously. The SPS spinning example initiates a simple method to use SPS as a new mechanism to delicately design the structure of the assembled 2D sheets. The revealed SPS mechanism opens a wide room to fabricate more distinct materials of 2D sheets for diverse applications.

Author contributions

Z. X. and C. G. conceived the research. F. F. C. carried out the experiment and characterizations and wrote this

manuscript. K. W. L., Y. J. L. and L. D. W. provided help with experimental details and drawing schematic diagrams. F. F. C. and L. D. W. fabricated the fibers based on the SPS wet-spinning method. F. F. C., K. W. L. and R. G. did the tensile tests of fibers. Y. C. Q. performed the display of fibers. C. W. S. help with the examination of DLS. All authors discussed the results and commented on the manuscript.

Data availability

The authors confirm that the data supporting the findings of this study are available within the article and its ESI.† Raw data that support the findings of this study are available from the corresponding authors upon reasonable request.

Conflicts of interest

There are no conflicts to declare.

Acknowledgements

This work is supported by the National Natural Science Foundation of China (52090030, 52090031 and 52272046), National Key Research and Development Program of China (2022YFA1205300, 2022YFA1205301), "Pioneer" and "Leading Goose" R&D Program of Zhejiang (2023C01190), the Natural Science Foundation of Zhejiang Province (No. LR23E020003), Hundred Talents Program of Zhejiang University (188020*194231701/113, 112300+1944223R3/003 and 112300+1944223R3/004), the Fundamental Research Funds for the Central Universities (226-2024-00074, 226-2024-00172 and 2023QZJH26), and Shanxi-Zheda Institute of New Materials and Chemical Engineering (No. 2022SZ-TD012 and 2022SZ-TD011). We thank XinNing Zhang from Testing and Analysis Center of Department of Polymer Science and Engineering, Zhejiang University, for the assistance in performing TEM. We thank Yi Guo and Yingying Zhang from Testing and Analysis Center of Department of Polymer Science and Engineering, Zhejiang University, for the assistance in performing SEM and CLSM.

References

1 X. Chen, X. Wu, H. Wu and M. Zhang, *Nat. Neurosci.*, 2020, **23**, 301–310.
2 M. I. Staples, C. Frazer, N. L. Fawzi and R. J. Bennett, *Nat. Microbiol.*, 2023, **8**, 375–386.
3 T. I. Lobling, O. Borisov, J. S. Haataja, O. Ikkala, A. H. Groschel and A. H. Muller, *Nat. Commun.*, 2016, **7**, 12097.
4 J. K. Phong, C. B. Cooper, L. Michalek, Y. Lin, Y. Nishio, Y. Shi, H. Gong, J. A. Vigil, J. Ilavsky, I. Kuzmenko and Z. Bao, *J. Mater. Chem. A*, 2024, **12**, 1145–1156.
5 C. Fernandez-Rico, S. Schreiber, H. Oudich, C. Lorenz, A. Sicher, T. Sai, V. Bauernfeind, S. Heyden, P. Carrara, L. Lorenzis, R. W. Style and E. R. Dufresne, *Nat. Mater.*, 2024, **23**, 124–130.
6 M. Wang, P. Zhang, M. Shamsi, J. L. Thelen, W. Qian, V. K. Truong, J. Ma, J. Hu and M. D. Dickey, *Nat. Mater.*, 2022, **21**, 359–365.
7 Z. Wang, M. Heck, W. Yang, M. Wilhelm and P. A. Levkin, *Adv. Funct. Mater.*, 2023, **34**, 2300947.
8 Z. Zhou, T. Liu, A. U. Khan and G. Liu, *Sci. Adv.*, 2019, **5**, eaau6852.
9 M. R. Krishnan, K. Y. Lu, W. Y. Chiu, I. C. Chen, J. W. Lin, T. Y. Lo, P. Georgopanos, A. Avgeropoulos, M. C. Lee and R. M. Ho, *Small*, 2018, **14**, e1704005.
10 H. W. Li and W. T. S. Huck, *Nano Lett.*, 2004, **4**, 1633–1636.
11 W. Li and M. Müller, *Prog. Polym. Sci.*, 2016, **54–55**, 47–75.
12 Z. Dong, H. Cui, H. Zhang, F. Wang, X. Zhan, F. Mayer, B. Nestler, M. Wegener and P. A. Levkin, *Nat. Commun.*, 2021, **12**, 247.
13 X. Shi, Y. Yao, J. Zhang, N. Corrigan and C. Boyer, *Small*, 2024, **20**, e2305268.
14 G. Y. Kim, S. Kim, J. Choi, M. Kim, H. Lim, T. W. Nam, W. Choi, E. N. Cho, H. J. Han, C. Lee, J. C. Kim, H. Y. Jeong, S. Y. Choi, M. S. Jang, D. Y. Jeon and Y. S. Jung, *Nano Lett.*, 2019, **19**, 6827–6838.
15 C. Lee and J. J. Kim, *Small*, 2013, **9**, 3858–3863.
16 N. Sary, F. Richard, C. Brochon, N. Leclerc, P. Leveque, J. N. Audinot, S. Berson, T. Heiser, G. Hadziioannou and R. Mezzenga, *Adv. Mater.*, 2010, **22**, 763–768.
17 X. Yu, K. Xiao, J. Chen, N. V. Lavrik, K. Hong, B. G. Sumpter and D. B. Geohegan, *ACS Nano*, 2011, **5**, 3559–3567.
18 L. Guo, Y. Wang and M. Steinhart, *Chem. Soc. Rev.*, 2021, **50**, 6333–6348.
19 K. V. Peinemann, V. Abetz and P. F. Simon, *Nat. Mater.*, 2007, **6**, 992–996.
20 A. P. Isfahani, M. Sadeghi, S. Nilouyal, G. Huang, A. Muchtar, M. M. Ito, D. Yamaguchi, E. Sivaniah and B. Ghalei, *J. Mater. Chem. A*, 2020, **8**, 9382–9391.
21 M. Radjabian and V. Abetz, *Prog. Polym. Sci.*, 2020, **102**, 101219.
22 C. Chen, J. Pan, J. Han, Y. Wang, L. Zhu, M. A. Hickner and L. Zhuang, *J. Mater. Chem. A*, 2016, **4**, 4071–4081.
23 H.-C. Chen, Y.-W. Su and K.-H. Wei, *J. Mater. Chem. A*, 2016, **4**, 2228–2235.
24 Y. Fu, B. Wang, J. Qu, Y. Wu, W. Ma, Y. Geng, Y. Han and Z. Xie, *Adv. Funct. Mater.*, 2016, **26**, 5922–5929.
25 D. Gao, J. Hollinger, A. A. Jahnke and D. S. Seferos, *J. Mater. Chem. A*, 2014, **2**, 6058–6063.
26 Y. Lee, M. P. Aplan, Z. D. Seibers, S. M. Kilbey, Q. Wang and E. D. Gomez, *J. Mater. Chem. A*, 2017, **5**, 20412–20421.
27 M. Sommer, S. M. Lindner and M. Thelakkat, *Adv. Funct. Mater.*, 2007, **17**, 1493–1500.
28 K. G. Cho, S. An, D. H. Cho, J. H. Kim, J. Nam, M. Kim and K. H. Lee, *Adv. Funct. Mater.*, 2021, **31**, 2102386.
29 Z. Shentu, Z. Zhang, J. Zhao, C. Chen, Q. Wu, L. Wang and X. Yan, *J. Mater. Chem. A*, 2021, **9**, 19619–19624.

30 W. Wu, H. Feng, L. Xie, A. Zhang, F. Liu, Z. Liu, N. Zheng and T. Xie, *Nat. Sustain.*, 2024, **7**, 804–811.
31 J. M. Eagan, J. Xu, R. Di Girolamo, C. M. Thurber, C. W. Macosko, A. M. LaPointe, F. S. Bates and G. W. Coates, *Science*, 2017, **355**, 814–816.
32 S. Deshpande and C. Dekker, *Curr. Opin. Colloid Interface Sci.*, 2021, **52**, 101419.
33 D. G. Lev, K. E. Gubbins, R. Radhakrishnan and M. Sliwinska-Bartkowiak, *Rep. Prog. Phys.*, 1999, **62**, 1573.
34 K. Binder, S. Puri, S. K. Das and J. Horbach, *J. Stat. Phys.*, 2010, **138**, 51–84.
35 P. Lesiak, K. Bednarska, W. Lewandowski, M. Wójcik, S. Polakiewicz, M. Bagiński, T. Osuch, K. Markowski, K. Orzechowski, M. Makowski, J. Bolek and T. R. Woliński, *ACS Nano*, 2019, **13**, 10154–10160.
36 Y. C. Lin, A. Motoyama, S. Kretschmer, S. Ghaderzadeh, M. Ghorbani-Asl, Y. Araki, A. V. Krasheninnikov, H. Ago and K. Suenaga, *Adv. Mater.*, 2021, **33**, e2105898.
37 G. Cicero, J. C. Grossman, E. Schwegler, F. Gygi and G. Galli, *J. Am. Chem. Soc.*, 2008, **130**, 1871–1878.
38 Z. Gao, N. Giovambattista and O. Sahin, *Sci. Rep.*, 2018, **8**, 6228.
39 R. A. L. Jones, L. J. Norton, E. J. Kramer, F. S. Bates and P. Wiltzius, *Phys. Rev. Lett.*, 1991, **66**, 1326–1329.
40 H. Tanaka, *Phys. Rev. Lett.*, 1994, **72**, 3690–3693.
41 S. M. Troian, *Phys. Rev. Lett.*, 1993, **71**, 1399–1402.
42 P. Wiltzius and A. Cumming, *Phys. Rev. Lett.*, 1991, **66**, 3000–3003.
43 J. Xia, J. Wang, Z. Lin, F. Qiu and Y. Yang, *Macromolecules*, 2006, **39**, 2247–2253.
44 Z. Xu and C. Gao, *Nat. Commun.*, 2011, **2**, 571.
45 Y. Jiang, Y. Wang, Z. Xu and C. Gao, *Acc. Mater. Res.*, 2020, **1**, 175–187.
46 P. Li, S. Wang, F. Meng, Y. Wang, F. Guo, S. Rajendran, C. Gao, Z. Xu and Z. Xu, *Macromolecules*, 2020, **53**, 10421–10430.
47 Y. Wang, S. Wang, P. Li, S. Rajendran, Z. Xu, S. Liu, F. Guo, Y. He, Z. Li, Z. Xu and C. Gao, *Matter*, 2020, **3**, 230–245.
48 S. Song, Y. Zhai and Y. Zhang, *ACS Appl. Mater. Interfaces*, 2016, **8**, 31264–31272.
49 X. Guo, L. Huang, X. Zhou, Q. Chang, C. Cao, G. Xiao and W. Shi, *Adv. Funct. Mater.*, 2020, **30**, 2003635.
50 Z. Liu, C. Liu, Y. Wang, M. Song, J. Guo, W. Wang and X. Gao, *Carbon*, 2024, **217**, 118655.
51 S. W. Kim, S.-N. Kwon and S. I. Na, *Composites, Part B*, 2019, **167**, 573–581.
52 T. Gabrys, B. Fryczkowska, D. Binias, C. Slusarczyk and J. Fabia, *Carbohydr. Polym.*, 2021, **254**, 117436.
53 L. Wang, B. Wang, Z. Wang, J. Huang, K. Li, S. Liu, J. Lu, Z. Han, Y. Gao, G. Cai, Y. Liu, Y. Chen, Y. Lin, Y. Liu, C. Gao and Z. Xu, *Nano Lett.*, 2023, **23**, 3352–3361.
54 L. Wang, K. Li, F. Chen, R. Guo, Y. Zhao, S. Liu, Y. Zhang, Z. Li, C. Shen, Z. Wang, X. Ming, Y. Liu, Y. Chen, Y. Liu, C. Gao and Z. Xu, *Nano Lett.*, 2024, **24**, 4256–4264.
55 G. Yang, Y. Yang, T. Chen, J. Wang, L. Ma and S. Yang, *ACS Appl. Nano Mater.*, 2022, **5**, 1068–1077.
56 J. Zhang, S. Luo, Y. Ma, R. Li, Y. Jin, L. Qiu and W. Zhang, *Chin. Chem. Lett.*, 2023, **34**, 107363.
57 N. Luo, Y.-Y. Zhang, H. Zhang, T.-L. Liu, Y. Wang, F. Chen and Q. Fu, *J. Mater. Chem. A*, 2024, **12**, 10359–10368.
58 R. Fontelo, R. L. Reis, R. Novoa-Carballal and I. Pashkuleva, *Adv. Healthc. Mater.*, 2024, **13**, e2301810.
59 X. Yang, H. Zhang, J. Zhao, Y. Liu, Z. Zhang, Y. Liu and X. Yan, *Chem. Eng. J.*, 2022, **450**, 138135.
60 A. Bianco, S. L. Burg, A. J. Parnell, C. M. Fernyhough, A. L. Washington, C. J. Hill, P. J. Smith, D. M. Whittaker, O. O. Mykhaylyk and J. P. A. Fairclough, *Langmuir*, 2017, **33**, 13303–13314.
61 M. Xu, Q. Cheng, L. Lin, J. Yang, Z. Liu, X. Yang, Q. Wang, F. Tang, A. He, C. Wang and X. Zhang, *Appl. Surf. Sci.*, 2023, **641**, 158537.
62 F. Schweitzer, *Phys. A*, 2021, **570**, 125687.
63 L. Kou and C. Gao, *Nanoscale*, 2013, **5**, 4370–4378.
64 X. Wang, J. Peng, Y. Zhang, M. Li, E. Saiz, A. P. Tomsia and Q. Cheng, *ACS Nano*, 2018, **12**, 12638–12645.
65 X. Hu, Z. Xu, Z. Liu and C. Gao, *Sci. Rep.*, 2013, **3**, 2374.